Article

pubs.acs.org/Biomac

Amphiphilic Peptides A_6K and V_6K Display Distinct Oligomeric Structures and Self-Assembly Dynamics: A Combined All-Atom and Coarse-Grained Simulation Study

Yunxiang Sun, Zhenyu Qian, Cong Guo, and Guanghong Wei*

State Key Laboratory of Surface Physics, Key Laboratory for Computational Physical Sciences (MOE), and Department of Physics, Fudan University, 220 Handan Road, Shanghai, 200433, China

Supporting Information

ABSTRACT: Amphiphilic peptides can self-assemble into ordered nanostructures with different morphologies. However, the assembly mechanism and the structures of the early assemblies prior to nanostructure formation remain elusive. In this study, we investigated the oligomeric structures of two amphiphilic heptapeptides A_6K and V_6K by all-atom explicit-solvent replica-exchange molecular dynamics (REMD) simulations, and then examined the assembly dynamics of large aggregates by coarse-grained (CG) MD simulations. Our 200 ns REMD simulations show that A_6K peptides predominantly adopt loosely packed disordered coil aggregates, whereas V_6K peptides mostly assemble into compact β-sheet-rich conformations, consistent with the signal measured experimentally in aqueous solution. Well-organized β-sheet-rich conformations, albeit with low population, are also populated for V_6K octamers, including bilayer β-sheets and β-barrels. These ordered β-sheet-rich conformations are observed for the first time for amphiphilic peptides. Our 10-μs CG-MD simulations on 200 peptide chains demonstrate that A_6K and V_6K peptides follow two different self-assembly processes, and the former form monolayer lamellas while the latter assemble into plate-like assemblies. CG-MD simulations also show that V_6K peptides display higher assembly capability than A_6K, in support of our all-atom REMD simulation results. Interpeptide interaction analyses reveal that the marked differences in oligomeric structures and assembly dynamics between A_6K and V_6K result from the subtle interplay of competition among hydrophobic, hydrogen-bonding, and electrostatic interactions of the two peptides. Our study provides structural and mechanistic insights into the initial self-assembly process of A_6K and V_6K at the molecular level.

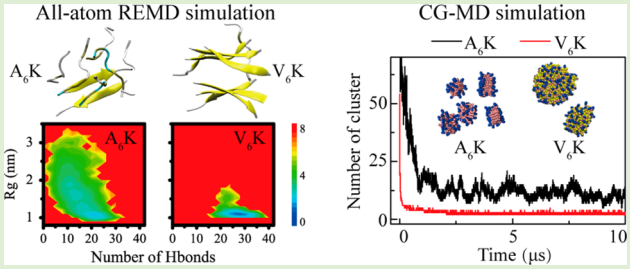

INTRODUCTION

A wide variety of peptides, including aromatic peptides, amyloid core peptides and amphiphilic peptides, can self-assemble into various ordered architectures, such as nanotubes, nanovesicles, micelles, bilayers, amyloid fibrils, tapes and ribbons.[1−16] Of particular interest are amphiphilic peptides, which have a polar head with one or more charged residues at the C-terminus and a hydrophobic tail with several consecutive hydrophobic residues at the N-terminus. They are an ideal model for understanding the ubiquitous phenomenon of self-assembly in nature, due to the advantages in molecular structure control and the easy manipulation of different forces resulting in well-defined architectures.[2,3] Their assembled structures can be readily tuned by tailoring peptide concentration, amino acid sequence, peptide length, and other solution conditions.[17,18] Their biocompatibility and tunable physicochemical properties makes the assembled nanostructures have potential applications in nanomedicine and nanotechnology. Although it is known that the typical major driving forces that regulate the self-assembly process of peptides are the noncovalent interactions including hydrogen bonding, van der Waals force, electrostatic interactions, hydrophobic interactions, and aromatic $\pi-\pi$ stacking,[1,19−21] the specific and quantitative roles of these interactions are not well understood. Development of basic rationales to link primary sequences with three-dimensional nanostructures will represent a major step toward the de novo design of peptide sequences targeting specific applications.[10]

Considerable efforts have been made to understand the relationship between the molecular architecture and the self-assemble nanostructure of amphiphilic peptides.[7,10,21−26] Previous studies have shown that amphiphilic peptides as short as 4 to 7 amino acid residues can self-assemble into nanostructures with different morphologies. Xu. et al. reported that ultrashort amphiphilic peptide L_3K self-organized into nanospheres with diameters of ∼10−15 nm, while I_3K self-assembled into nanotubes with diameters of ∼10 nm.[27] Secondary structure studies revealed that in aqueous solution I_3K mainly adopted β-sheet conformation, but L_3K lacked any significant β-sheet structure.[27,28] These results indicate that minor differences in the structure of leucine (L) and isoleucine

Received: June 26, 2015
Revised: August 20, 2015
Published: August 24, 2015

DOI: 10.1021/acs.biomac.5b00850
Biomacromolecules 2015, 16, 2940−2949

Table 1. Setup Details of All-Atom and Coarse-Grained Simulations[a]

peptide model	system	box size (nm^3)	# of peptides	# of water molecules	concentration (mM)
all-atom	A_6K	5.7 × 5.7 × 5.7	8	5554	72
	V_6K	5.7 × 5.7 × 5.7	8	5471	72
coarse-grained	A_6K	16 × 16 × 16	200	22801	81
	V_6K	16 × 16 × 16	200	22296	81

[a]For each system, we list peptide model, name of the system, simulation box size, number of peptide chains, number of water molecules, and peptide concentration.

(I) result in marked differences in the self-assembled nanostructures. Han et al. designed and synthesized three sets of short amphiphilic peptides (I_3K, LI_2K, and L_3K; L_3K, L_4K, and L_5K; I_3K, I_4K, and I_5K) and investigated how I and L residues affected the self-assembly of these peptides in aqueous solution.[27] These results revealed a strong tendency of I groups to promote the formation of β-sheet and the subsequent nanostructure formation; the L groups have a weak tendency to form β-sheet structure, but increasing the number of hydrophobic residues in amphiphilic peptides L_nK (n = 3−5) could enhance β-sheet formation.[27,28] Han et al. also studied the effect of residue hydrophobicity on the self-assembly of the amphiphilic peptides (G_6K, A_6K, V_6K) in bulk solution and at the silica/water interface. Transmission electron microscope (TEM) imaging showed that in aqueous solution, A_6K and V_6K molecules respectively assembled into nanofibers and nanostacks, but no aggregated structure was observed for G_6K due to weak hydrophobic character.[1] Recently, Wang et al. examined the secondary structure and the self-assembly of A_6K and V_6K peptides in aqueous solution. Circular dichroism (CD) spectrum of these two peptides respectively revealed a random coil conformation and a typical β-sheet structure. Their atomic force microscopy experiments showed that A_6K could self-assemble into nanotubes, while V_6K self-organized into nanostacks.[29]

In spite of extensive experimental studies, the initial step of amphiphilic peptide self-assembly, especially the structures of the early assemblies and their possible link with the morphology of the experimentally observed nanostructures are still unclear. Unveiling the structural nature of assemblies formed in the early stage of peptide self-assembly is of great importance for understanding the molecular mechanism of nanostructure formation at microscopic level. An increasing number of studies reported that oligomers (2−20-mers) formed in the early stage of peptide self-assembly exist only transiently and at low concentrations, thus it is challenging to characterize their high-resolution structure experimentally.[30−32] In this study, the structures of small octamers and the self-assembly processes of large aggregates of the two amphiphilic peptides A_6K and V_6K were investigated using molecular dynamics (MD) simulations. As self-assembly usually occurs in a microsecond time scale or even longer,[33−35] it is thus computationally expensive to perform all-atom simulations at constant temperature. As an alternative, in this study, enhanced sampling methods, all-atom replica exchange molecular dynamics (REMD) simulation and coarse-grained molecular dynamics (CG-MD) simulation, were used to investigate respectively peptide oligomerization and large assembly formation. The reason for selecting eight chains in our all-atom REMD simulations is as follows. Previous all-atom MD simulation studies reported that a bilayer β-sheet consisting of eight peptide chains is stable to be a seed for the fibril growth of several amyloid-forming peptides, including alanine-rich peptides AGAAAAGA and AAAAAAAA,[36] amyloid-β fragment of KLVFFAE,[37] and NFGAIL.[38] As A_6K and V_6K peptides have similar amino acid length and composition as these peptides, they may need eight chains to form a nucleus. Our 200 ns all-atom explicit-solvent REMD simulations on the self-assembly of eight peptide chains revealed that A_6K peptides adopt predominantly random coil conformations, with a very weak tendency to form β-sheet structure, whereas V_6K peptides have a much higher propensity to form β-sheet conformation. A_6K peptides form mainly disordered coil aggregates, whereas V_6K mostly assemble into β-sheet-rich octamers, including ordered bilayer β-sheets, β-barrels, double β-barrels, as well as disordered octamers. Our 10-μs coarse-grained MD simulations on 200 peptide chains demonstrate that V_6K peptides have a higher assembly capability than A_6K peptides. During the self-assembly process, monolayer lamellas are observed for A_6K molecules, whereas round plate-like assemblies are sampled for V_6K peptides. The possible link of these ordered β-sheet-rich octamers and large assemblies with the experimentally observed nanostructures are discussed.

MATERIAL AND METHODS

Peptide Models. A_6K (AAAAAAK) and V_6K (VVVVVVK) peptides were both capped by the ACE (CH_3CO) group at the N-terminus and the NH_2 group at the C-terminus, as done experimentally by Wang et al.[29] Eight A_6K or V_6K peptide chains were investigated in the all-atom REMD simulations. Two hundred A_6K or V_6K peptide chains were studied in the CG-MD simulations. All-atom and coarse-grained models of A_6K and V_6K peptides are given in Figure S1 (Supporting Information). The net charge of the peptide is +1 at neutral pH. Counterions (Cl^-) were added to neutralize the system.

All-Atom REMD Simulations. The REMD method is an enhanced sampling simulation method[39−41] which consists in running multiple MD simulations in parallel of the same system, but at different temperatures. At regular time intervals, exchanges of conformations at different temperatures were attempted and eventually swapped according to metropolis criteria. This method is useful for simulating complex problems such as amyloid peptide aggregation[42,43] and peptide self-assembly.[44] All-atom explicit REMD simulations were performed using the GROMACS software package[45] with the Amber99SB force field.[46] Eight A_6K or V_6K peptide chains, with random conformations for each chain, were initially placed randomly in a 5.7 × 5.7 × 5.7 nm^3 box filled with simple point change (SPC) water molecules. There are 5554 and 5471 water molecules in A_6K and in V_6K system, respectively. The peptide concentration for both A_6K and V_6K systems is 72 mM. This peptide concentration, which is much higher than experimental one, is used to accelerate the assembly process and decrease computational cost. The choice of this high peptide concentration is also motivated by recent REMD studies by de Groot group[47] and our group.[48] The REMD study by de Groot group on the oligomerization of the VEALYL peptide from insulin at four different concentrations (3.3, 8.3, 16.6, and 83 mM) demonstrated that the final structures approached ordered aggregates with steric-zipper-like structural features, irrespective of the initial peptide concentration.[47] The REMD study by our group on Aβ(16−

DOI: 10.1021/acs.biomac.5b00850
Biomacromolecules 2015, 16, 2940−2949

22) octamer showed that quite similar β-sheet content (47.3% vs 46.6%) was obtained at two different peptide concentrations (33.97 and 64.74 mM).[48] Setups details of all-atom REMD simulations are given in Table 1. The REMD simulation was carried out in the NPT ensemble using 48 replicas, each of 200 ns duration, at temperatures exponentially spaced between 300 and 440 K. The temperature lists for the two systems are given in the Supporting Information. The swap time between two neighboring replicas is 2 ps. The acceptance ratio is ~17%. Periodic boundary conditions were applied in all three directions. Bond length of peptides and water molecules were constrained, respectively, using the LINCS[49] and SETTLE[50] algorithms, allowing an integration time step of 2 fs. Nonbonded pair lists were updated every five integration steps. The protein and nonprotein (water and counterions) groups were separately coupled to an external heat bath with a relaxation time of 0.1 ps using a velocity rescaling coupling method.[51] The pressure was kept at 1 bar using the Parrinello−Rahman method[52] with a coupling time constant of 1.0 ps. Electrostatic interactions were treated with the particle mesh Ewald method[53] with a real space cutoff of 1.0 nm. The van der Waals interactions were calculated using a cutoff of 1.4 nm.

Coarse-Grained MD Simulations. The assembly dynamics of large aggregates of A_6K or V_6K peptides was studied using the Martini coarse-grained model[54,55] implemented in GROMACS 4.5.3[56] software. This force field was parametrized in a systematic way, combining top-down and bottom-up strategies: nonbonded interactions are based on the reproduction of experimental partitioning free energies between polar and apolar phases of a large number of chemical compounds, whereas bonded interactions are derived from reference all-atom simulations.[57−60] The MARTINI model was also extensively parametrized for amino acids[54,58−60] and the interaction strength between side chain beads and backbone beads closely match atomistic reference models.[58,60] This CG model is widely used as an effective model for studying peptide self-assembly[19,33,34,61,62] and it extends the accessible simulation time scale significantly by employing a 4:1 heavy-atom/CG-bead mapping and a reduced water model. Each CG water bead corresponds to four water molecules. The MARTINI V2.2P polarizable force field[58] was used to model peptides and water molecules.

It is noted that secondary structure changes of proteins cannot be modeled in Martini force field, and explicit hydrogen bonds are also absent in this CG model, although changes in tertiary structure are unrestricted.[54,59,60] To initiate a simulation using MARTINI model, the secondary structure should be first assigned to the peptide chains, and the assigned secondary structure remains fixed during the simulation.[54,55] In our CG-MD simulations, the secondary structure assignment of A_6K and V_6K is based on our all-atom REMD simulation results of the octamers (more details about the secondary structure assignment are given in the Results and Discussion section). Two hundred A_6K or V_6K peptide chains were initially placed randomly in a 16.0 × 16.0 × 16.0 nm^3 cubic box and solvated with water. There are 22801 and 22296 polarizable water molecules in the A_6K and V_6K systems, respectively. Peptide concentration in the CG-MD simulations is 81 mM, very close to the concentration of 72 mM in all-atom REMD simulations. Setup details of CG-MD simulations are given in Table 1. A 10-μs CG-MD simulation was performed in NPT ensemble for both systems. This Martini CG model not only reduces the number of degrees of freedom significantly, but also allows a large integration time step between 20 and 40 fs in the simulation, thus assuring a more efficient sampling scheme. Here we used a time step of 30 fs. A temperature of 300 K was kept with a coupling constant of 0.3 ps, and a pressure of 1 atm was maintained with a coupling constant of 3 ps via the Berendsen coupling methods.[52] Electrostatic and van der Waals (vdW) interactions were used in their shifted forms with a cutoff at a distance of 1.2 nm. The vdW interaction was shifted from 0.9 to 1.2 nm and the electrostatic interaction was shifted from 0.0 to 1.2 nm. The neighbor-list was updated every 10 steps with a distance cutoff of 1.4 nm.

Analysis Methods. Trajectory analysis was performed with our in-house developed codes and the tools implemented in GROMACS-4.5.3[56] software package. For both A_6K and V_6K systems, the data in the first 120 ns REMD trajectories were discarded to remove the bias of the initial states. For the all-atom REMD simulation data, the secondary structure of the peptide was identified using the DSSP program.[63] The average percentage of each secondary structure was calculated by only considering the middle five residues for each peptide chain as the two terminal residues are always in random coil conformation, irrespective of secondary structure of the peptide. The end-to-end distance of each peptide chain and the percentage of various sizes of β-sheet were calculated. The end-to-end distance refers to the minimum distance between the heavy atoms in ACE group at the N-terminus and the NH_2 group at the C-terminus. The size of a β-sheet is the number of strands in an n-stranded β-sheet; e.g., the β-sheet size of a two-stranded β-sheet is two. Two chains are considered to form a β-sheet if (i) at least two consecutive residues in each chain visit the β-strand state and (ii) they have at least two hydrogen bonds (H-bonds). One H-bond is taken as formed if the N···O distance is less than 0.35 nm and the N−H···O angle is greater than 150°. We did a two-step cluster analysis. First, cluster analysis was performed by Daura algorithm[64] using a C_α root-mean-square deviation (RMSD) cutoff of 0.3 nm. The central conformation of each cluster was put into a pool. Second, for all the central conformations in the pool, we calculated the chain-independent C_α-RMSD for each pair of central conformations by neglecting the identifier of each peptide chain, as we have done previously for Aβ(16−22) octamer.[65] A two-dimensional (2D) free energy surface was constructed using $-RT \ln P$(Rg, H-bond number), where P(Rg, H-bond number) is the probability of a conformation having a certain value of Rg and H-bond number. Here, Rg and H-bond number denote the radius of gyration of the octamer and the total number of hydrogen bonds (including intra- and intermolecular H-bonds), respectively. The interpeptide interactions were analyzed by the residue−residue contact probabilities. Here, a contact was defined when the heavy atoms of two nonsequential side chains (or main chains) come within 0.65 nm. For the CG simulation data, two peptide chains were considered to be in the same cluster when their minimum distance is within 0.65 nm. The VMD program was used for trajectory visualization and for graphical structure analysis.

RESULTS AND DISCUSSION

Before analyzing the simulation data, the convergence of the two REMD simulations was examined by comparing the following several parameters within two different time intervals using the 120−160 ns and 160−200 ns data for both A_6K and V_6K systems at 300 K. These parameters include the probability density function (PDF) of end-to-end distance of each peptide chain in the oligomers, and the average propensity of each secondary structure over the five residues in the middle of the amino acid sequence, and the secondary structure contents (including coil, β-sheet, β-bridge, bend, turn and helix) of each amino acid residue. As shown in Figure S2 (Supporting Information), the end-to-end distance distribution curves within the two independent time intervals (120−160 ns and 160−200 ns) overlap very well both for the two systems. The average secondary structure (including coil, β-sheet, β-bridge, bend, turn and helix) contents over the middle five residues within the two time intervals in Figure S3 (Supporting Information) are quite similar for both systems, with a difference for each secondary structure content being less than 0.01. The dominant secondary structure (coil and β-sheet) propensities of each residue within the two different time intervals are also close to each other (Figure S4). We also checked the sampling efficiency by following the time evolution of temperature swapping of one representative replica in temperature space. As shown in Figure S5 (Supporting Information), the representative replica of A_6K system (A) and V_6K system (B) visited the full temperature space several

DOI: 10.1021/acs.biomac.5b00850
Biomacromolecules 2015, 16, 2940−2949

times during the 200 ns REMD simulation, indicating the replica was not trapped in one single temperature or one aggregated state. Other replicas show similar sampling behavior (data not shown). Taken together, all these results provide strong evidence that the two REMD simulations have reasonably converged within 200 ns. Unless specified, all the REMD simulation results presented below are based on the last 80 ns (t = 120−200 ns) simulation data generated at 300 K.

A_6K and V_6K peptides in the oligomers display marked difference in peptide dimension and secondary structure propensity. The end-to-end distance probability distribution for both A_6K and V_6K peptides in the oligomers are presented in Figure 1A. A broad ensemble of states is observed

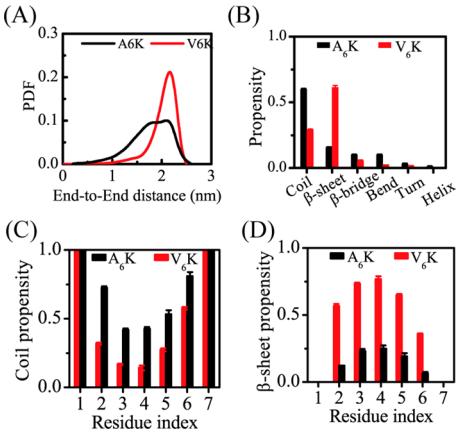

Figure 1. Analyses of peptide dimension and secondary structure propensity of A_6K and V_6K peptides in oligomers. (A) Probability distribution of the end-to-end distance of each peptide chain. (B) Average propensity of each secondary structure over the middle five alanine/valine residues in the amino acid sequence of A_6K/V_6K peptide. (C) Coil propensity of each residue. (D) β-sheet propensity of each residue.

between 1.0 and 2.5 nm for A_6K peptide (black curve), while the ensemble shifts between 1.5 and 2.5 nm for V_6K peptide (red curve), and there is a sharp peak centered around 2.2 nm. These data indicate that V_6K peptide in the oligomers is much more extended than A_6K peptide.

The average propensity of secondary structure over the middle five residues and the dominant secondary structure (β-sheet and coil) probability of each residue are shown in Figure 1B−D. For A_6K peptide, the probabilities of helical and turn structures are negligible, and the peptide mostly adopts coil conformation (roughly 60.1% population) and, to a much lesser extent, β-sheet (15.6%), β-bridge (10.1%), and bend (10.0%) conformations (Figure 1B). Compared to the secondary structure content of A_6K peptide, the coil content of V_6K is reduced to 29.0% and the β-sheet percentage increases significantly to 61.5%. The percentage of other secondary structures of V_6K is insignificant. Figure 1C,D gives the probabilities of dominant secondary structures (β-sheet and coil) as a function of residue index. The β-sheet probability in Figure 1D showed that valine residues V2−V5 in V_6K aggregates have the highest probability (about 57−77%) to adopt β-sheet conformations with respect to other residues. The coil propensity of these residues ranges from 12% to 56%. The five alanine residues (A2−A6) in the middle of A_6K amino acid sequence have a β-sheet propensity of 5−24%, while their coil propensity is 43−81%. These data, together with the end-to-end distance distribution in Figure 1A, demonstrate that A_6K peptides mostly adopt collapsed coil conformations, and to a much lesser extent, β-sheet conformations, while V_6K peptides have a larger propensity to adopt extended β-sheet conformations. This is consistent with the CD spectrum of A_6K and V_6K peptides in aqueous solution reported recently by Wang et al.[29]

Of particular interest is that the β-sheet propensity of valine residue V2/V3 (with a probability of 57%/73%) close to the N-terminus is much higher than that of V6/V5 (36%/65%) close to the C-terminus. This higher β-sheet propensity of V2 (57%) versus V6 (36%) and V3 (73%) versus V5 (65%) probably results from the higher hydrophobicity at N-terminal region due to the cooperative hydrophobic effect (see below for more detailed discussion).

β-Sheets in A_6K and V_6K Oligomers Have Different Size Distribution and Parallel:Antiparallel Ratio. After comparing the secondary structure propensity of the two systems, we further calculated the probability of β-sheet sizes (see Figure 2A). We found that the dominant β-sheet formed

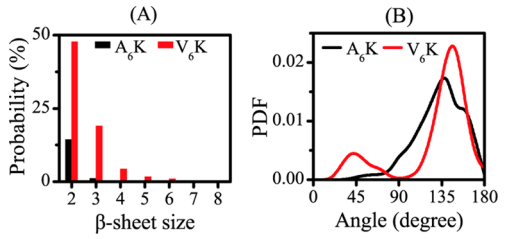

Figure 2. β-Sheet structure analysis for A_6K and V_6K systems: (A) probability of different sizes of β-sheet; (B) the distribution of angle between two neighboring β-strands in all sizes of β-sheets.

by A_6K is two-stranded β-sheet, with a probability of ∼15%, while other sizes of β-sheets are insignificant. The probability of two-stranded β-sheet in V_6K system is greatly enhanced (48%). Three-, four-, five-, and six-stranded β-sheets are also observed, having a probability of 19%, 4% and 2%, and 1% respectively, indicating V_6K peptides can form larger β-sheets than A_6K peptides.

To explore the parallel and antiparallel alignments of β-strands in β-sheets, we computed the probability distribution of angle between two neighboring β-strands in all size of β-sheets (Figure 2B). The calculated angles between A_6K β-strands are in the range of 90−180 deg, indicating A_6K peptides mainly form antiparallel β-sheets. The angle distribution curve of V_6K shows two peaks: a dominant peak centered at 150 deg (in the range of 90−180 deg) and a minor peak centered at 45 deg (in the range of 20−90 deg). These data imply that V_6K peptides mostly adopt antiparallel β-sheets, but also have certain probability to form parallel β-sheets. The calculated parallel:antiparallel β-sheet ratio in V_6K β-sheets is about 1:5, while the ratio in A_6K β-sheets is approximately 0.

A_6K β-Sheets Are Mostly Stabilized by Hydrogen-Bonding Interaction, while V_6K β-Sheets Are Stabilized by Both Hydrophobic and Hydrogen-Bonding Interactions. To probe the crucial interactions stabilizing the β-sheets structures, we calculated the pairwise residue main-chain−main-chain (MC−MC) and side-chain−side-chain (SC−SC) contact probabilities for β-sheet structures in A_6K and V_6K oligomers. Figure 3 demonstrates that the contact probability maps of A_6K and V_6K β-sheets display similar

DOI: 10.1021/acs.biomac.5b00850
Biomacromolecules 2015, 16, 2940−2949

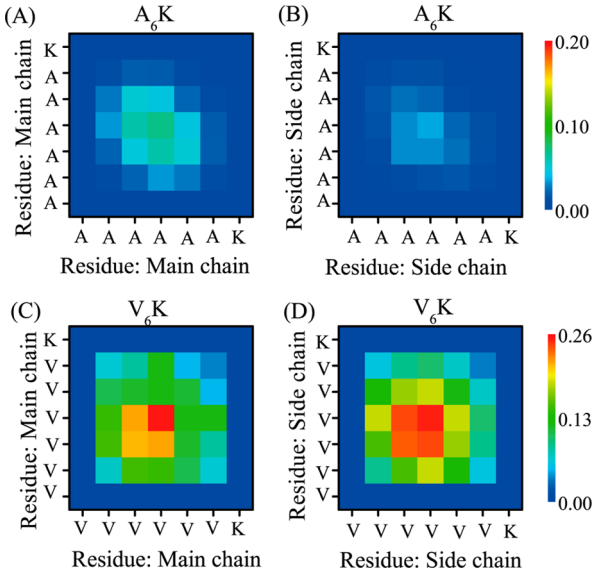

Figure 3. Main-chain−main-chain (MC−MC) and side-chain−side-chain (SC−SC) contact probability maps for peptide chains forming β-sheet structures in A_6K oligomer (A,B) and V_6K oligomer (C,D).

interaction patterns, but the contact probabilities are significantly different: the MC-MC and SC-SC contact probabilities of V_6K are much higher than those of A_6K. Figure 3A,B shows that with respect to other residue pairs, A4−A4 and A3−A4 pairs have the highest MC−MC contact probabilities, 10% vs 8%, whereas the highest SC-SC contact probability is only 4% between A4−A4 pair. These data indicate that mainchain hydrogen-bonding interaction plays a dominant role on the antiparallel β-sheet formation of A_6K peptides. It can be seen from Figure 3C,D that the MC−MC contact probabilities between V3−V3 (with a contact probability of 22%), V3−V4 (23%), and V4−V4 (26%) residue pairs are almost the same as the SC−SC contact probabilities between V3−V3 (24%), V3−V4 (25%), and V4−V4 (26%) pairs. This similarity between the MC−MC and SC−SC contact probabilities imply that V_6K β-sheets are stabilized by both hydrophobic and hydrogen-bonding interactions. An interesting observation in the contact probability map is that V3−V3 pair display much higher MC−MC and SC−SC contact probabilities than V5−V5 pair, and V2−V2 pair has much higher MC−MC and SC−SC contact probabilities than V6−V6 pair. This finding reflects the important role of N-terminal hydrophobic valine residues on the β-sheet formation of V_6K peptide. It is expected from the amino acid sequence that residues V2 and V3 in the N-terminal region have a more hydrophobic environment than the C-terminal residues V5 and V6. For example, V2 has two first-nearest-neighboring hydrophobic residues (V1 and V3), while V6 has only one first-nearest-neighboring hydrophobic residue (V5), and the other first-nearest-neighboring residue (K7) is hydrophilic. Compared to the C-terminal valine residues, the much stronger hydrophobic interaction between the N-terminal valine residues reveals a cooperative hydrophobic effect. The same behavior is observed for A_6K peptides, albeit to a much lesser extent. These results provide an explanation for the higher β-sheet propensity of N-terminal residues observed in Figure 1D.

The MC−MC and SC−SC contact probability maps of A_6K and V_6K also provide an explanation for the observation of the solely antiparallel β-sheet formation of A_6K peptide and both parallel and antiparallel β-sheet formation of V_6K peptide. Given the weak hydrophobicity and the short amino acid length of A_6K peptide, it is unlikely that interpeptide MC−MC hydrogen-bonding and SC−SC hydrophobic interactions can provide enough stabilization to outweigh the electrostatic repulsion between positively charged lysine residues. Therefore, an antiparallel β-strand arrangement, in which the distance between the positive charges of lysine residues is maximized, is favored. An increase in hydrophobicity in V_6K peptide makes the SC−SC hydrophobic interaction and backbone interchain H-bonding overwhelm the electrostatic repulsion between the charged groups of lysine side chains, thus providing the chance for parallel β-sheet formation as well.

A_6K Peptides Mainly Self-Assemble into Loosely Packed Disordered Coil Aggregates, while Substituting Valine for Alanine Leads to Compact β-Sheet-Rich Octamers. To investigate the three-dimensional conformational states of A_6K and V_6K oligomers, we first performed a RMSD-based cluster analysis for 8000 conformations sampled for each system at 300 K using the procedure described in the Analysis Methods subsection. Using a C_α-RMSD cutoff of 0.3 nm, the conformations of A_6K and V_6K oligomers are separated into 1336 and 87 clusters, respectively. The centers of the top nine most populated clusters and their populations are shown in Figure 4. These clusters represent 21.8% and 62.9% of all

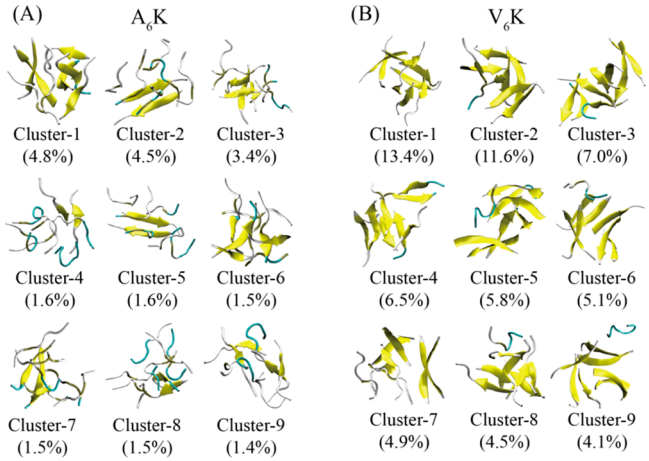

Figure 4. Representative conformations of the first nine most-populated clusters for A_6K (A) and V_6K (B) octamers. The corresponding population of each cluster is given in the parentheses.

conformations of A_6K and V_6K oligomers, respectively. The observation that the percentages of the nine clusters of A_6K are much smaller than those of V_6K reveals the low similarity and high diversity of conformations of A_6K octamers compared to V_6K octamers. It can be seen from this Figure 4A that A_6K octamers are mostly in disordered coil conformations, while V_6K peptides are predominantly β-sheet-rich conformations, with most of them containing two- and three-stranded β-sheets.

To have an overall view of the conformational distribution of A_6K and V_6K oligomers, we plotted in Figure 5 the two-dimensional free energy landscape (or potential of mean force, PMF) as a function of Rg and H-bond number. As shown in Figure 5, the free energy surface of A_6K oligomers is broad and shallow, with the number of H-bonds ranging from 2 to 30 and the Rg ranging from 0.9 to 3.2 nm. The large range of (number of H-bonds, Rg) values observed for A_6K oligomers indicate that eight A_6K peptide chains can form various sizes of

DOI: 10.1021/acs.biomac.5b00850
Biomacromolecules 2015, 16, 2940−2949

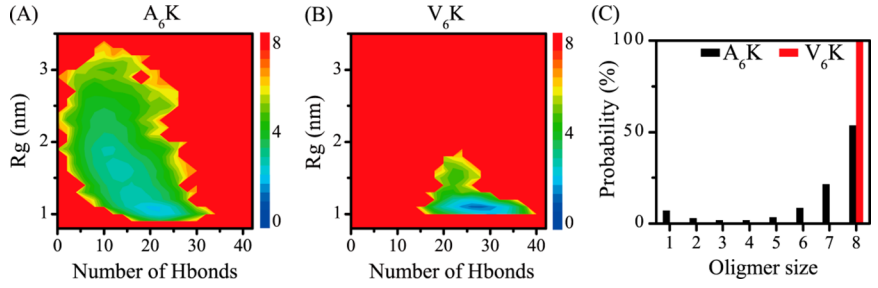

Figure 5. Analysis of conformational space of A_6K and V_6K oligomers. Free energy landscape (in kcal/mol) of A_6K (A) and V_6K (B) oligomers as a function of the total number of H-bonds (number of H-bonds) and radius of gyration (Rg). (C) Probability of different sizes of oligomers.

oligomers with different β-sheet content. In contrast, the free energy landscape of V_6K oligomers is rather narrow and deep, with the number of H-bonds and Rg being respectively in the range of 15−38 and 1.0−1.7 nm. The large number of H-bonds and small Rg imply that eight V_6K peptide chains form compact octamers.

To further determine the oligomer sizes formed by eight A_6K/V_6K peptide chains, we presented the probability distribution of the different oligomers in Figure 5C. It can be seen that A_6K peptides form predominantly octamer and heptamer, with a probability of 54% and 22%, respectively. The probabilities of forming monomer, dimer, trimer, tetramer, pentamer, and hexamer are 6%, 3%, 2%, 2%, 3%, 8%, respectively. These data demonstrate that eight A_6K peptide chains can form various sizes of oligomers ranging from dimers to octamers due to the weak hydrophobicity of alanine residues. This result also indicates that in the early stage of self-assembly, A_6K is in equilibrium between mostly monomer, hexamer, heptamer, and octamer. The formation of various sizes of A_6K oligomers explains the observation of large cluster number of A_6K oligomers. In contrast, eight V_6K peptide chains self-assemble into solely compact octamers (with a probability of ~100%). These results reveal that V_6K peptide has a higher self-assembly capability than A_6K.

Although the V_6K octamers primarily adopt disordered β-sheet-rich conformations, they can also sample well-organized structures, albeit with a very low probability. Figure 6 shows all the ordered β-sheet structures. Based on their topology, these structures can be classified into two types: bilayer β-sheet and β-barrel. Different sizes of bilayer β-sheets are denoted by $m + n$ (Figure 6A,B), where m and n respectively represent the m- and n-stranded β-sheets forming the bilayer. Four sizes of bilayer β-sheets are observed for V_6K octamers, and they are 3 + 3, 4 + 4, 5 + 3, and 4 + 4 bilayer β-sheets. The two sheets are parallel, while the β-strands in each sheet are mostly in antiparallel alignment. The four different β-barrels include 5-stranded open β-barrel (open-B5), 5-stranded closed β-barrel (closed-B5), 6-stranded open β-barrel (open-B6) and double 5-stranded open β-barrel (open-dB5) sharing a common curved three-stranded β-sheet.

These ordered β-sheet-rich octamers, which are observed for the first time for amphiphilic peptides, are particularly interesting as they might serve as a building block for large ordered nanostructure formation. Interestingly, a recent MD study by Yifat et al. reported that β-hairpin structure is the building block of hydrogel formed by a 20-residue MAX1 peptide.[66] The bilayer β-sheets observed in our REMD simulations could grow into long nanofibers and large nanosheets depending on the lateral interactions between different faces of β-sheets.[67] In terms of hydrophobicity, the

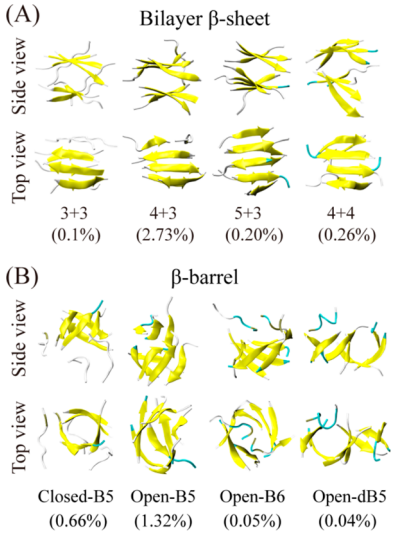

Figure 6. Representative V_6K octamers containing ordered bilayer β-sheets and β-barrels, shown in two different views: top view and side view. (A) Four different sizes of bilayer β-sheets. (B) Four different β-barrels, including single β-barrels and double β-barrels. The probability of each structure is given in the parentheses.

two faces of a V_6K β-sheet are symmetric, it is very likely that V_6K bilayer β-sheets would grow into large nanosheets. The double 5-stranded open β-barrel could grow into a long 1D ordered nanostructure consisting of multiple 5-stranded open β-barrels via monomer addition along the hydrogen-bond direction through a dock-lock mechanism.[68] As the population of double open β-barrel (0.04%) is much lower than bilayer β-sheets (3.29%), large nanosheets would be the most possible self-assembly product of V_6K. Different from V_6K octamers, ordered β-sheet structures are not seen for A_6K octamers. This indicates that eight A_6K peptide chains are not sufficient for ordered β-sheet formation, and a large number of peptide chains is necessary, due to the weak hydrophobicity of alanine residues. These ordered β-sheet-rich octamers have also been reported for amyloid core sequences in previous computational and experimental studies.[65,69,70] This observation is consistent with a recent experimental study showing that aliphatic peptides display similar self-assembly to amyloid core sequences.[17]

Self-Assembly Dynamics of Large Number of A_6K and V_6K Peptide Chains Using Coarse-Grained Simulations at a Microsecond Time Scale. After characterizing the structures and the free energy landscapes of A_6K and V_6K oligomers, we further explore the assembly process of large number of peptide chains using the Martini coarse-grained

DOI: 10.1021/acs.biomac.5b00850
Biomacromolecules 2015, 16, 2940−2949

model at a μs time scale. Considering the REMD results that the vast majority (84.4%) of A_6K chains are in coil conformations and the vast majority (61.5%) of V_6K chains are in β-sheet conformations, we preset, for simplicity, all of the A_6K/V_6K chains in coil/β-sheet conformation in our CG MD simulations. A 10-μs CG-MD simulation was carried out both for A_6K and V_6K systems, each system consisting of 200 peptide chains. To monitor the self-assembly dynamics, we calculated the normalized solvent accessible surface area (SASA) and the number of clusters as a function of time. The time evolution of normalized SASA in Figure 7A shows

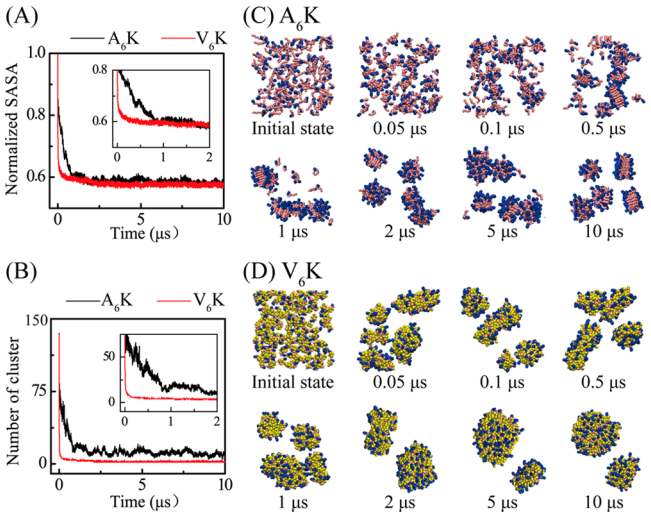

Figure 7. Analysis of the self-assembly process of 200 A_6K and V_6K peptide chains in a 10-μs CG-MD trajectory. Time evolution of normalized SASA (A) and number of clusters (B). The insets in panels A and B give the time evolution of the normalized SASA and number of clusters within the first of 2 μs. Snapshots at several time points are given in panel C for A_6K and panel D for V_6K systems. In each snapshot, the backbone beads of each residue are in pink, and the side chain beads of V and K are respectively in yellow and blue. Water molecules and Cl^- ions are not shown for clarity.

that the SASA of A_6K system initially decreases quickly, and reaches to its final value of 0.6 within the first 0.8 μs. An increase in hydrophobicity leads to a much fast assembly process of V_6K. Within only 0.25 μs, the SASA of V_6K system is reduced to its final value of 0.6.

Similar time evolution behavior is also seen for the number of cluster (Figure 7B). The number of A_6K cluster is rapidly reduced to 13 within the first 0.8 μs, then gradually decreases in the next 4 μs, and fluctuates between 5 and 15 in the last 5 μs. Such a large fluctuation of cluster number in the last 5 μs of the simulation is mostly ascribed to the weak hydrophobicity of alanine residues. The number of V_6K cluster decreases much faster, and it reaches 5 at 0.25 μs; afterward it slowly changes and keeps around 2 during the last 5 μs. These data show that the self-assembly of V_6K is much faster than that of A_6K and V_6K has higher self-assembly capability than A_6K, consistent with our all-atom REMD simulations on the octamer.

To intuitively show the assembly process, we present the snapshots at eight time points in Figure 7C,D. Starting from a state with a random distribution of 200 A_6K peptide chains in the water box (Figure 7C), peptides come together to form many small clusters within the first 0.1 μs. At t = 0.5 μs, some clusters merge into a few monolayer lamellas, with the backbone beads of alanine residues in β-sheet-like alignment and the side chain beads of lysine residues pointing to the solvent. The thickness of the lamellas is ~1.9 nm, which is comparable with the length of an extended A_6K peptide chain. With the increase of simulation time, more peptides chains join to the monolayer lamellas and more lamellar assemblies are formed (see the snapshot at t = 2 μs). However, these monolayer lamellas are not stable due to the weak hydrophobic interactions between alanine residues. Peptides at the edge of the lamellas can continuously dissociate and reassociate, and individual peptides are observed during the full 10-μs assembly process, indicating the slow assembly process of A_6K peptides. Some of the isolated peptides are in extended states, while others are in collapsed states (see the snapshots at t = 1 and 5 μs). These lamellas evolve with time, and five monolayer lamellas are formed at t = 10 μs. Three different views of the snapshot at t = 10 μs are given in Figure 8A. A previous cryo-

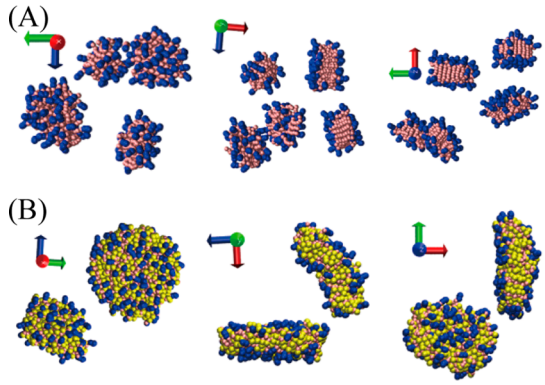

Figure 8. Final snapshots (at t = 10 μs) for (A) A_6K and (B) V_6K assemblies in three different views. We use the same color code as in Figure 7. For clarity, water molecules and counterions are not shown.

transmission electron microscopy (cryo-TEM) study by Ziserman et al.[71] reported that, in aqueous solution, a synthesized peptide amphiphilie (referred to as C12-β12) self-assembled into different nanostructures when the incubation time was different: fibers within minutes, twisted ribbon at 1 day, coil helical ribbon at 1 week, unclosed tube at 4 weeks, and finally closed nanotube at four months. Similar morphological transformation process of (β)A(β)AKLVFF assemblies was also observed by Adamcik et al.[72] Small-angle neutron scattering and wide-angle X-ray diffraction experiments by Ziserman et al.[71] demonstrated that the fundamental unit of the fibers, ribbons, and nanotubes of C12-β12 is a monolayer lamella formed by the peptide amphiphilie. Based on the study by Ziserman et al, we propose that the A_6K monolayer lamellas observed in our simulation could progress into fibers and nanotubes during different time durations much longer than microseconds. This could help reconcile conflicting experimental observation on the morphology of A_6K nanostructures reported in the TEM study (nanofiber) by Han et al[1] and that in the AFM study (nanotube) by Wang et al.[29] Thus, the observation of different nanostructures in the two studies probably results from the different incubation time of A_6K peptide solution.

The self-assembly process of V_6K peptides (Figure 7D) is dramatically different from A_6K peptides. Starting from a state with a random distribution of 200 V_6K peptide chains in the simulation box, large clusters with different shapes are formed

DOI: 10.1021/acs.biomac.5b00850
Biomacromolecules 2015, 16, 2940−2949

within only 0.05 μs due to strong hydrophobic interactions between valine residues. Afterward some of these clusters start to fuse and then form two larger aggregates at 2 μs. Through reorganization of the peptide chains, the two aggregates transform into round plate-like nanostructures at 5 μs, which maintain during the last 5 μs. Three different views of the two round nanoplate generated at t = 10 μs are given in Figure 8B. The diameters of these two plate-like assemblies are 8.6 and 7.6 nm, respectively. Noting that the plates are not exactly round in shape, but they are usually extended in one direction. The diameter of the plate is the average of the diameters along the long and short principle axes. In the nanoplate, the backbone beads of all residues and most of the side chain beads of valine residues are buried inside the nanoplate, while the polar side chain beads of lysine residues are exposed to solvent. The morphology of the plate-like V_6K assemblies observed in our simulation is in good agreement with the AFM and TEM image of V_6K nanostructures observed previously.[1,29]

We also compared the CG data with the all-atom data by analyzing K−K distance distributions for A_6K/V_6K aggregates generated in all-atom (AA) and coarse-grained (CG) simulations. As seen from Figure S6, two dominant peaks are observed in all of the K−K distance distribution curves. For A_6K system (see Figure S6A), the two all-atom K−K distance distribution peaks at 1.52 and 2.42 nm correspond to two different out-of-register antiparallel β-sheet organizations. The CG K−K distance distribution peak centered at 1.50 nm corresponds to an in-register antiparallel alignment of two A_6K peptides, consistent with the antiparallel alignment of all-atom A_6K peptides. Similar results are observed in Figure S6B for all-atom and CG K−K distribution curves of V_6K system. It is noted that the peak at 0.95/0.96 nm in Figure S6A,B corresponds to the K−K distance between a peptide and its second-nearest neighboring peptide in the A_6K/V_6K assemblies. The three small peaks at 0.6, 0.8, and 1.3 nm in Figure S6B correspond to respectively one-, two-, and three-residue-shift out-off-register parallel β-sheet alignments. Overall, the CG K−K distance distribution curve is consistent with the all-atom curve for both A_6K and V_6K systems, although differences are also seen in the all-atom and CG curves due to the different sizes of assemblies under-studied and the different level of models used.

CONCLUSIONS

In summary, we have investigated the oligomeric structures and the self-assembly process of large aggregates of two amphiphilic peptides, A_6K and V_6K, by performing all-atom REMD simulations and coarse-grained MD simulations. We find that eight A_6K peptide chains mainly form loosely packed oligomers ranging from dimers to octamers, and an increase in hydrophobicity leads to solely compact V_6K octamers, indicating a higher assembly ability of V_6K peptide. A_6K peptide chains predominantly adopt random coil structure and to a much lesser extent of β-sheet conformation, while substituting alanine with valine leads to a dramatic increase of β-sheet content and a decrease of coil content. Due to the electrostatic repulsion between the lysine residue and the low hydrophobicity of alanine residues, β-strands in A_6K β-sheet are solely in antiparallel alignment. An increase in hydrophobicity overwhelms the electrostatic repulsion between positively charged lysine residue, which facilitates the formation of both antiparallel and parallel β-sheets for V_6K peptides. Interpeptide contact probability analysis based on all-atom simulation data shows that A_6K β-sheets are mostly stabilized by hydrogen-bonding interaction, while V_6K β-sheets are stabilized by both hydrophobic and hydrogen-bonding interactions (such a difference cannot be explicitly represented in the Martini model due to the lack of explicit hydrogen bonds and the coarse-graining of backbone and side-chain beads). Conformational analysis shows that A_6K oligomer adopt collapsed disordered coil aggregates, while V_6K mostly self-organize into disordered β-sheet-rich octamers, and, to a much lesser extent, ordered bilayer β-sheets and β-barrels. These ordered β-sheet-rich octamers, which are observed for the first time for amphiphilic peptide, are quite similar to the ordered β-sheet-rich oligomers formed by amyloid core sequences such as Aβ(16−22) peptide. This observation indicates that bilayer β-sheets and β-barrels might be typical conformations of peptide oligomers. Ordered β-sheet structures are not observed for A_6K octamers, implying that eight A_6K peptide chains are not sufficient for ordered β-sheet formation due to weak hydrophobic character. Our 10-μs coarse-grained MD simulations on 200 peptide chains show that A_6K and V_6K peptides display distinct assembly pathways and the assembly process of V_6K is much faster than A_6K. V_6K peptides can quickly aggregate into larger assemblies, while the self-assembly process of A_6K peptides is much slower and peptide chains can easily dissociate from the formed aggregates. Multiple A_6K peptide chains can self-organize into monolayer lamellas, while V_6K peptides self-assemble into plate-like structures, consistent with the AFM images observed previously. Our study provides molecular insights into self-assembly process of A_6K and V_6K peptides at a microscopic level, which might be helpful for the design of novel nanostructure formed by amphiphilic peptides for targeted applications.

ASSOCIATED CONTENT

Supporting Information

Additional data provided, including the temperature list of REMD simulation for A_6K and V_6K systems, and six supplementary figures. These figures present all-atom and coarse-grained models of A6K and V6K peptides, and convergence check for the REMD runs of A_6K and V_6K systems (including the probability density function (PDF) of end-to-end distance of all chains, secondary structure propensity as a function of each secondary structure, and secondary structure contents of each residue) at 300 K using two time windows, 120−160 ns, 160−200 ns, the time evolution of temperature swapping of one representative replica in temperature space, and the K−K distance distribution for A_6K/V_6K aggregates generated in all-atom and coarse-grained simulations. The Supporting Information is available free of charge on the ACS Publications website at DOI: 10.1021/acs.biomac.5b00850.

(PDF)

AUTHOR INFORMATION

Corresponding Author

*E-mails: ghwei@fudan.edu.cn.

Notes

The authors declare no competing financial interest.

ACKNOWLEDGMENTS

G.W. acknowledges the financial support from the NSF of China (Grant No. 91227102 and 11274075). Simulations were

DOI: 10.1021/acs.biomac.5b00850
Biomacromolecules 2015, 16, 2940−2949

performed at the National High Performance Computing Center of Fudan University.

REFERENCES

(1) Han, S. Y.; Xu, W. W.; Cao, M. W.; Wang, J. Q.; Xia, D. H.; Xu, H.; Zhao, X. B.; Lu, J. R. *Soft Matter* **2012**, *8* (3), 645−652.
(2) Altunbas, A.; Sharma, N.; Lamm, M. S.; Yan, C.; Nagarkar, R. P.; Schneider, J. P.; Pochan, D. J. *ACS Nano* **2010**, *4* (1), 181−188.
(3) Holmstrom, S. C.; King, P. J.; Ryadnov, M. G.; Butler, M. F.; Mann, S.; Woolfson, D. N. *Langmuir* **2008**, *24* (20), 11778−11783.
(4) Adler-Abramovich, L.; Gazit, E. *Chem. Soc. Rev.* **2014**, *43* (20), 6881−6893.
(5) Colombo, G.; Soto, P.; Gazit, E. *Trends Biotechnol.* **2007**, *25* (5), 211−218.
(6) Mehta, A. K.; Lu, K.; Childers, W. S.; Liang, Y.; Dublin, S. N.; Dong, J.; Snyder, J. P.; Pingali, S. V.; Thiyagarajan, P.; Lynn, D. G. *J. Am. Chem. Soc.* **2008**, *130* (30), 9829−9835.
(7) Gazit, E. *Chem. Soc. Rev.* **2007**, *36* (8), 1263−1269.
(8) Kim, H. J.; Kim, T.; Lee, M. *Acc. Chem. Res.* **2011**, *44* (1), 72−82.
(9) Dehsorkhi, A.; Hamley, I. W. *Soft Matter* **2014**, *10* (11), 1660−1664.
(10) Zhang, S. *Acc. Chem. Res.* **2012**, *45* (12), 2142−2150.
(11) Balbach, J. J.; Ishii, Y.; Antzutkin, O. N.; Leapman, R. D.; Rizzo, N. W.; Dyda, F.; Reed, J.; Tycko, R. *Biochemistry* **2000**, *39* (45), 13748−13759.
(12) Gorbitz, C. H. *Chem. - Eur. J.* **2001**, *7* (23), 5153−5159.
(13) Reches, M.; Gazit, E. *Science* **2003**, *300* (5619), 625−627.
(14) Reches, M.; Porat, Y.; Gazit, E. *J. Biol. Chem.* **2002**, *277* (38), 35475−35480.
(15) Petkova, A. T.; Ishii, Y.; Balbach, J. J.; Antzutkin, O. N.; Leapman, R. D.; Delaglio, F.; Tycko, R. *Proc. Natl. Acad. Sci. U. S. A.* **2002**, *99* (26), 16742−16747.
(16) Adler-Abramovich, L.; Vaks, L.; Carny, O.; Trudler, D.; Magno, A.; Caflisch, A.; Frenkel, D.; Gazit, E. *Nat. Chem. Biol.* **2012**, *8* (8), 701−706.
(17) Lakshmanan, A.; Cheong, D. W.; Accardo, A.; Di Fabrizio, E.; Riekel, C.; Hauser, C. A. E. *Proc. Natl. Acad. Sci. U. S. A.* **2013**, *110* (2), 519−524.
(18) Zhao, X.; Pan, F.; Xu, H.; Yaseen, M.; Shan, H.; Hauser, C. A.; Zhang, S.; Lu, J. R. *Chem. Soc. Rev.* **2010**, *39* (9), 3480−3498.
(19) Guo, C.; Luo, Y.; Zhou, R. H.; Wei, G. H. *Nanoscale* **2014**, *6* (5), 2800−2811.
(20) Wang, J.; Han, S. Y.; Meng, G.; Xu, H.; Xia, D. H.; Zhao, X. B.; Schweins, R.; Lu, J. R. *Soft Matter* **2009**, *5* (20), 3870−3878.
(21) Yan, X. H.; Zhu, P. L.; Li, J. B. *Chem. Soc. Rev.* **2010**, *39* (6), 1877−1890.
(22) de la Rica, R.; Matsui, H. *Chem. Soc. Rev.* **2010**, *39* (9), 3499−3509.
(23) Hamley, I. W. *Angew. Chem., Int. Ed.* **2007**, *46* (43), 8128−8147.
(24) Vauthey, S.; Santoso, S.; Gong, H.; Watson, N.; Zhang, S. *Proc. Natl. Acad. Sci. U. S. A.* **2002**, *99* (8), 5355−5360.
(25) von Maltzahn, G.; Vauthey, S.; Santoso, S.; Zhang, S. U. *Langmuir* **2003**, *19* (10), 4332−4337.
(26) Nagai, A.; Nagai, Y.; Qu, H.; Zhang, S. *J. Nanosci. Nanotechnol.* **2007**, *7* (7), 2246−2252.
(27) Xu, H.; Wang, Y. M.; Ge, X.; Han, S. Y.; Wang, S. J.; Zhou, P.; Shan, H. H.; Zhao, X. B.; Lu, J. A. R. *Chem. Mater.* **2010**, *22* (18), 5165−5173.
(28) Han, S.; Cao, S.; Wang, Y.; Wang, J.; Xia, D.; Xu, H.; Zhao, X.; Lu, J. R. *Chem. - Eur. J.* **2011**, *17* (46), 13095−13102.
(29) Wang, Q. R.; Yu, J.; Zhang, X.; Liu, D. J.; Zheng, J. H.; Pan, Y.; Lin, Y. J. *RSC Adv.* **2013**, *3* (8), 2784−2793.
(30) Bitan, G.; Teplow, D. B. *Acc. Chem. Res.* **2004**, *37* (6), 357−364.
(31) Eisenberg, D.; Jucker, M. *Cell* **2012**, *148* (6), 1188−1203.
(32) Arosio, P.; Knowles, T. P.; Linse, S. *Phys. Chem. Chem. Phys.* **2015**, *17* (12), 7606−7618.
(33) Marrink, S. J.; Tieleman, D. P. *Chem. Soc. Rev.* **2013**, *42* (16), 6801−6822.
(34) Guo, C.; Luo, Y.; Zhou, R.; Wei, G. *ACS Nano* **2012**, *6* (5), 3907−3918.
(35) Klein, M. L.; Shinoda, W. *Science* **2008**, *321* (5890), 798−800.
(36) Ma, B. Y.; Nussinov, R. *Protein Sci.* **2002**, *11* (10), 2335−2350.
(37) Rohrig, U. F.; Laio, A.; Tantalo, N.; Parrinello, M.; Petronzio, R. *Biophys. J.* **2006**, *91* (9), 3217−3229.
(38) Wu, C.; Lei, H. X.; Duan, Y. *Biophys. J.* **2004**, *87* (5), 3000−3009.
(39) Sugita, Y.; Okamoto, Y. *Chem. Phys. Lett.* **1999**, *314* (1−2), 141−151.
(40) Okamoto, Y. *J. Mol. Graphics Modell.* **2004**, *22* (5), 425−439.
(41) Nadler, W.; Hansmann, U. H. *J. Phys. Chem. B* **2008**, *112* (34), 10386−10387.
(42) Qi, R.; Luo, Y.; Ma, B.; Nussinov, R.; Wei, G. *Biomacromolecules* **2014**, *15* (1), 122−131.
(43) Levine, Z. A.; Larini, L.; LaPointe, N. E.; Feinstein, S. C.; Shea, J. E. *Proc. Natl. Acad. Sci. U. S. A.* **2015**, *112* (9), 2758−2763.
(44) Mu, X.; Eckes, K. M.; Nguyen, M. M.; Suggs, L. J.; Ren, P. *Biomacromolecules* **2012**, *13* (11), 3562−3571.
(45) Lindahl, E.; Hess, B.; van der Spoel, D. *J. Mol. Model.* **2001**, *7* (8), 306−317.
(46) Hornak, V.; Abel, R.; Okur, A.; Strockbine, B.; Roitberg, A.; Simmerling, C. *Proteins: Struct., Funct., Genet.* **2006**, *65* (3), 712−725.
(47) Matthes, D.; Gapsys, V.; de Groot, B. L. *J. Mol. Biol.* **2012**, *421* (2−3), 390−416.
(48) Xie, L.; Lin, D.; Luo, Y.; Li, H.; Yang, X.; Wei, G. *Biophys. J.* **2014**, *107* (8), 1930−8.
(49) Hess, B.; Bekker, H.; Berendsen, H. J. C.; Fraaije, J. G. E. M. *J. Comput. Chem.* **1997**, *18* (12), 1463−1472.
(50) Miyamoto, S.; Kollman, P. A. *J. Comput. Chem.* **1992**, *13* (8), 952−962.
(51) Bussi, G.; Donadio, D.; Parrinello, M. *J. Chem. Phys.* **2007**, *126* (1), 014101−014107.
(52) Berendsen, H. J. C.; Postma, J. P. M.; Vangunsteren, W. F.; Dinola, A.; Haak, J. R. *J. Chem. Phys.* **1984**, *81* (8), 3684−3690.
(53) Darden, T.; York, D.; Pedersen, L. *J. Chem. Phys.* **1993**, *98* (12), 10089−10092.
(54) Monticelli, L.; Kandasamy, S. K.; Periole, X.; Larson, R. G.; Tieleman, D. P.; Marrink, S. J. *J. Chem. Theory Comput.* **2008**, *4* (5), 819−834.
(55) Marrink, S. J.; Risselada, H. J.; Yefimov, S.; Tieleman, D. P.; de Vries, A. H. *J. Phys. Chem. B* **2007**, *111* (27), 7812−7824.
(56) Van der Spoel, D.; Lindahl, E.; Hess, B.; Groenhof, G.; Mark, A. E.; Berendsen, H. J. C. *J. Comput. Chem.* **2005**, *26* (16), 1701−1718.
(57) Yesylevskyy, S. O.; Schafer, L. V.; Sengupta, D.; Marrink, S. J. *PLoS Comput. Biol.* **2010**, *6* (6), e1000810.
(58) de Jong, D. H.; Singh, G.; Bennett, W. F. D.; Arnarez, C.; Wassenaar, T. A.; Schafer, L. V.; Periole, X.; Tieleman, D. P.; Marrink, S. J. *J. Chem. Theory Comput.* **2013**, *9* (1), 687−697.
(59) Singh, G.; Tieleman, D. P. *J. Chem. Theory Comput.* **2011**, *7* (7), 2316−2324.
(60) de Jong, D. H.; Periole, X.; Marrink, S. J. *J. Chem. Theory Comput.* **2012**, *8* (3), 1003−1014.
(61) Thota, N.; Ma, Y. J.; Jiang, J. W. *RSC Adv.* **2014**, *4* (105), 60741−60748.
(62) Emamyari, S.; Kargar, F.; Sheikh-hasani, V.; Emadi, S.; Fazli, H. *Eur. Biophys. J.* **2015**, *44* (4), 263−276.
(63) Kabsch, W.; Sander, C. *Biopolymers* **1983**, *22* (12), 2577−2637.
(64) Daura, X.; Gademann, K.; Jaun, B.; Seebach, D.; van Gunsteren, W. F.; Mark, A. E. *Angew. Chem., Int. Ed.* **1999**, *38* (1−2), 236−240.
(65) Li, H.; Luo, Y.; Derreumaux, P.; Wei, G. *Biophys. J.* **2011**, *101* (9), 2267−2276.
(66) Miller, Y.; Ma, B. Y.; Nussinov, R. *J. Phys. Chem. B* **2015**, *119* (2), 482−490.
(67) Dai, B.; Li, D.; Xi, W.; Luo, F.; Zhang, X.; Zou, M.; Cao, M.; Hu, J.; Wang, W. Y.; Wei, G. H.; Zhang, Y.; Liu, C. *Proc. Natl. Acad. Sci. U. S. A.* **2015**, *112* (10), 2996−3001.
(68) Nguyen, P. H.; Li, M. S.; Stock, G.; Straub, J. E.; Thirumalai, D. *Proc. Natl. Acad. Sci. U. S. A.* **2007**, *104* (1), 111−116.

DOI: 10.1021/acs.biomac.5b00850
Biomacromolecules 2015, 16, 2940−2949

(69) Kato, M.; Han, T. N. W.; Xie, S. H.; Shi, K.; Du, X. L.; Wu, L. C.; Mirzaei, H.; Goldsmith, E. J.; Longgood, J.; Pei, J. M.; Grishin, N. V.; Frantz, D. E.; Schneider, J. W.; Chen, S.; Li, L.; Sawaya, M. R.; Eisenberg, D.; Tycko, R.; McKnight, S. L. *Cell* **2012**, *149* (4), 753−767.
(70) Xie, L. G.; Luo, Y.; Wei, G. H. *J. Phys. Chem. B* **2013**, *117* (35), 10149−10160.
(71) Ziserman, L.; Lee, H. Y.; Raghavan, S. R.; Mor, A.; Danino, D. *J. Am. Chem. Soc.* **2011**, *133* (8), 2511−2517.
(72) Adamcik, J.; Castelletto, V.; Bolisetty, S.; Hamley, I. W.; Mezzenga, R. *Angew. Chem., Int. Ed.* **2011**, *50* (24), 5495−5498.

DOI: 10.1021/acs.biomac.5b00850
Biomacromolecules 2015, 16, 2940−2949